Chemical Physics Letters 595–596 (2014) 156–166

Contents lists available at ScienceDirect

Chemical Physics Letters

journal homepage: www.elsevier.com/locate/cplett

# Spontaneous insertion of carbon nanotube bundles inside biomembranes: A hybrid particle-field coarse-grained molecular dynamics study

Edita Sarukhanyan [a,b,1], Antonio De Nicola [a,c,1], Danilo Roccatano [b], Toshihiro Kawakatsu [d], Giuseppe Milano [a,c,*]

[a] Dipartimento di Chimica e Biologia, Università di Salerno, I-84084 via Ponte don Melillo, Fisciano (SA), Italy
[b] Jacobs University Bremen, Campus Ring 1, D-28759, Germany
[c] IMAST Scarl-Technological District in Polymer and Composite Engineering, P.le Bovio 22, 80133 Napoli (NA), Italy
[d] Department of Physics, Tohoku University, Aoba, Aramaki, Aoba-ku, Sendai 980-8578, Japan

ARTICLE INFO

*Article history:*
Received 5 November 2013
In final form 31 January 2014
Available online 8 February 2014

ABSTRACT

The processes of CNTs bundle formation and insertion/rearrangement inside lipid bilayers, as models of cellular membranes, is described and analyzed in details using simulations on the microsecond scale. Molecular Dynamics simulations employing hybrid particle-field models (MD–SCF) show that during the insertion process lipid molecules coat bundles surfaces. The distortions of bilayers are more pronounced for systems undergoing to insertion of bundles made of longer CNTs. In particular, when the insertion occurs in perpendicular orientation, adsorption of lipids on CNTs surfaces promotes a transient poration. This result suggests mechanism of membrane disruption operated by bundles causing the formation of solvent-rich pockets.



## 1. Introduction

Due to their ability to cross cellular membranes, carbon nanotubes (CNTs) have been proposed to be exploited as nano-transporters for drugs or other biologically active molecules inside the cell [1]. After being discovered, CNTs have attracted scientific attention due to their outstanding properties and characteristics [1]. Indeed, their ability to cross cell membranes [2] opens innumerable possibilities for biomedical applications [3,4]. Their large surface area allows attachment (of chemical or physical nature) of drug molecules [5–7] and the empty core of the CNTs provides an opportunity to exploit them as nano-containers for drug [8,9] or any desired biologically active molecule encapsulation [10,11]. For this reason, several experimental studies have been performed in order to understand the pathways of internalization [12–19]. Al-Jamal et al. [12] have studied the cellular mechanism of functionalized Multi Walled CNTs (MWCNTs) by 3D electron tomography imaging. Two types of cells – epithelial lung carcinoma cells (A549) and human monocyte-derived macrophages (HMMs) have been considered for the interactions with $NH^{3+}$ functionalized MWCNTs. The results of the study suggest that the CNT internalizations can occur either by direct piercing of the membrane of single nanotubes or by the wrapping of the nanotube by lipids of the cell membrane [12]. The study of the mechanism of uptake of single walled CNTs (SWCNTs) by HMMs has been performed by Porter et al. [14] using confocal microscopy and transmission electron microscopy (TME) techniques. This Letter suggested endocytosis and passive diffusion as possible mechanism. However, in a different study by Yaron [19] and coworkers based on confocal Raman spectroscopy and fluorescence lifetime imaging (FLIM) have found that the internalization of SWCNT occurs by only endocytosis and not for passive diffusion through membrane. The SWCNTs used in all these studies were non covalently functionalized by Pluronic F127 (PF-127). It was found that PF-127–SWCNT were localized in endosomes while interacting with HeLa cells [1,20].

A molecular understanding of the mechanism of interaction of carbon CNTs with cellular membranes would help the development of CNTs based systems for targeted drug delivery. So far, experimental methods can provide for these systems only limited information at the molecular scale level. For this reason, several simulation studies involving CNT and lipid bilayers have been reported [17,18,21–27]. Molecular dynamics simulations based on

* Corresponding author at: Dipartimento di Chimica e Biologia, Università di Salerno, I-84084 via Ponte don Melillo, Fisciano (SA), Italy.
*E-mail address:* gmilano@unisa.it (G. Milano).
[1] Both of these authors contributed equally to this work.

http://dx.doi.org/10.1016/j.cplett.2014.01.057
0009-2614/

atomistic or coarse-grained models can provide detailed information on these processes. Unfortunately, the processes of insertion and rearrangement even of a single CNT into a lipid bilayer are slow if compared with the timescales reachable by atomistic simulations. For this reason, often special techniques (biased simulations such as steered molecular dynamics or free energy scans along a given reaction coordinate) aimed to explore this process are needed. Atomistic simulations have been employed to perform steered molecular dynamics (SMD) [17] and static scans of environmental free energy [18] to study the insertion of very short (typical lengths were 2 nm [17] and from 3 to 6 nm [18]) single CNTs into a lipid bilayer. Parthasarathi et al. built up atomistic models where CNTs are embedded in the lipid bilayer from the beginning of the simulations and investigated perturbations caused by the presence of single CNTs and their bundles (having CNTs length of 6 nm) on a lipid bilayer [21]. Moreover, the insertion process of a small graphene nanosheet into a lipid bilayer structure has been studied using atomistic simulations [22].

In order to explore length and time scales relevant to these problems, a number of simulation studies using coarse-grained (GC) models have been used to characterize the process of spontaneous insertion of several nanosized objects into lipid bilayers. In particular, hydrophobic nanopores [23], fullerenes [24,25], SWCNT [18], and the piercing mechanism of a single CNT into a model membrane [26] have been studied using CG models. The mechanism of spontaneous insertion of short pristine CNTs has been recently studied by Lelimousin and Sansom using molecular dynamics simulations of CG models [27]. In particular, in this Letter the spontaneous insertion of single CNTs of different types (single and multi-walled) and sizes (length ranging from 2 to 10 nm) inside model membranes has been characterized. Baoukina et al. studied using CG models the insertion of single CNTs and bundles formed by short CNTs (having lengths up to 6.5 nm) by molecular dynamics simulations [28].

With these precedents, the aim of the present Letter is to characterize the insertion mechanism of bundles formed by aggregation of CNTs of different lengths (ranging from 4 to 20 nm). In particular, differently from the results reported in Ref. [27] this Letter is focused on the mechanism of insertion of CNTs bundles. The relevance of these systems is related to the main difficulty in the use of CNT in nanomedicine associated with their hydrophobicity and tendency to aggregate into bundles. In fact, for practical applications, such aggregates have cytotoxic effect and even cause cell death in dose dependent manner [29]. Systems size and simulations timescales suitable to treat and to observe the spontaneous insertion process of CNTs bundles can be still feasible for coarse-grained models still close to atomistic (typically one bead corresponds to four non hydrogen atoms, 4:1 mapping), as the ones reported in this Letter, if non-bonded interactions are treated using a Self Consistent Field (SCF) theory approach having models based on a hybrid particle-field (PF) representation [30]. Using the hybrid methodology, differently from traditional coarse-grained models limited to the study of the insertion of a single CNT [27] or small bundles made of short CNTs [28], it has been possible to study the entire process of spontaneous insertions of bundles made of longer CNTs (10 and 20 nm).

The Letter is organized as follows, in the Section 2, the simulation methodology based on MD and hybrid PF representation is briefly introduced and the models used in the present Letter are described. In the results and discussion section the process of CNTs bundle formation is described and then the process of insertion and rearrangement of bundles formed by CNTs of length ranging from 4 to 20 nm is described and analyzed in details. Supporting information section contains: a more detailed description of the MD–SCF hybrid approach, more details about models, their parameters and some additional results.

## 2. Models and methods

### 2.1. Simulation methodology

The simulations reported in this Letter have been performed using a hybrid particle-field scheme combining Molecular Dynamics (MD) and Self Consistent Field theory.

This hybrid approach, due to its computational efficiency, is gaining popularity for simulations of several soft matter systems including nanocomposites [31] and biomembranes [32–35]. Particle and field representations of coarse-grained models of homopolymer and block copolymer systems have been used in the single chain in mean field (SCMF) method introduced by Daoulas and Muller [36,37]. More recently, the MD method has been combined with SCF description, which hereafter we call 'MD–SCF' approach. In particular, an implementation suitable for the treatment of atomistic force fields and/or specific CG models has been reported and validated [30,38].

The coarse-grained models adopted in this Letter for lipids have been extensively described and validated in two previous papers [39,40] and recently reviewed in the framework of efficient strategies for biomembranes modeling [33]. The main advantage of hybrid MD–SCF scheme is that the most computationally expensive part of the MD simulations, i.e. the evaluation of the non-bonded force between atoms of different molecules, is replaced by the evaluation of forces between independent molecules with an external potential. In the particle-field approximation, the external potential $V(\mathbf{r})$ corresponds to the non bonded potential between one particle and the remaining ones in the range of the pair wise potential. The external potential $V(\mathbf{r})$, calculated from the values of the density at position $\mathbf{r}$ is:

$$V_K(\mathbf{r}) = \frac{\delta W[\{\phi_K(\mathbf{r})\}]}{\delta \phi_K(\mathbf{r})} = k_B T \sum_{K'} \chi_{KK'} \phi_{K'}(\mathbf{r}) + \frac{1}{\kappa}\left(\sum_K \phi_K(\mathbf{r}) - 1\right). \quad (1)$$

A derivation of Eq. (1) and the approximations behind it are reported in the Supporting information section. The first addend of Eq. (1) corresponds to the interaction of a single particle of type $K$ with the fields due to particles of type $K'$. The second addend is the so-called incompressibility condition keeping the density homogenous in the space.

In order to connect particle and field models, for the proposed hybrid MD–SCF scheme, it is necessary to obtain a smooth coarse-grained density function directly from the particle positions. This function is obtained by implementing a mesh based approach which is suitable to obtain also the density derivatives needed to calculate forces. The details of the implementation of this approach and a complete derivation is reported in references [30,38]. In order to help the reader, in the Supporting information section a brief overview of the theoretical scheme and its implementation is included.

### 2.2. Simulation details

Simulations reported here have been performed using the parallelized version of the OCCAM code [41]. The compositions of each simulated system are reported in Table 1.

All simulations have been performed with velocity Verlet algorithm using a time step of 0.03 ps in the *NVT* ensemble by keeping the temperature constant at 325 K using Andersen thermostat with a collision frequency of 5 $ps^{-1}$. The calculations of the fields have been performed using a grid with a resolution of 0.705 nm and an update frequency of 300 steps. This choice of the grid size guarantees good reproduction of lipid properties [39,40]. Furthermore the value 0.705 nm is almost half of the CNTs diameters, in this way excluded volume interactions between CNTs is properly

**Table 1**
Systems composition.

| System | Box length [$x = y = z$] (nm) | DWCNT length (nm) | No. of DPPC | No. of CG-water Beads* | No. of DWCNT | Total no. of particles | Simulation time (μs) | Initial position of bundle[a] (nm) |
|---|---|---|---|---|---|---|---|---|
| I | 12.0000 | 4.6 | – | 14051 | 6 | 14844 | 0.27 | – |
| II | 16.3521 | 4.6 | 832 | 27829 | 6 | 38605 | 3.0 | 4.5 |
| III | 32.7042 | 10.0 | 3319 | 267088 | 6 | 308500 | 1.2 | 2.5[b]<br>4.0[c] |
| IV | 32.7042 | 20.0 | 3319 | 265541 | 6 | 308537 | 1.2 | 2.5[b]<br>10[c] |

* A single CG water bead corresponds to 4 real water molecules.
[a] Distance between centre of mass and first layer.
[b] Parallel orientation with respect to the bilayer.
[c] Perpendicular orientation with respect to the bilayer.

described by the incompressibility condition (second addend of Eq. (1)).

Additional information about the models and their parameters is reported in the Supporting information section.

## 3. Results and discussion

### 3.1. Bundle formation

A system of six nanotubes of length 4.6 nm in water has been simulated (system I in Table 1). The initial configuration was made by placing CNTs randomly in the simulation box, but avoiding overlapping between them, and, hence by adding water beads. In Figure 1, together with the behavior of the sum over all particles of the first addend of the external potential $V(r)$ (first addend of Eq. (1), in the following this will be named particle-field potential) several snapshots are shown, in the following. A first sudden aggregation, corresponding to a drop in the particle-field potential, between closest CNTs is obtained. The first snapshots of Figure 1 show some disordered aggregations between two or three CNTs. In particular, unstable (small contact surface) and stable (large contact surface) pairs between CNTs can be identified. During the simulation it is possible to observe unstable pairs dissociating or evolving through stable pairs. Stable pairs, when formed, are able to promote aggregation of further CNTs until, in almost 250 ns, an ordered bundle is formed. It is interesting to see that when stable contacts are formed and contemporary dissociations of other pairs do not occur this corresponds to fast drops in the particle-field potential (for instance from the second to the third configuration of Figure 1).

Larger bundle or bundles having longer CNTs show similar behaviors to the ones reported here. Ordered bundles configurations employed in the simulations of the next sections for systems having CNTs long 10 and 20 nm (systems III and IV) have been constructed from the beginning of the simulation and equilibrated in water. In particular, bundles have been pre-equilibrated in systems containing only water (no bilayer). These equilibrated structures have been used as starting points for the simulations described in this Letter. The initial distances and other information about the simulated systems are reported in Table 1.

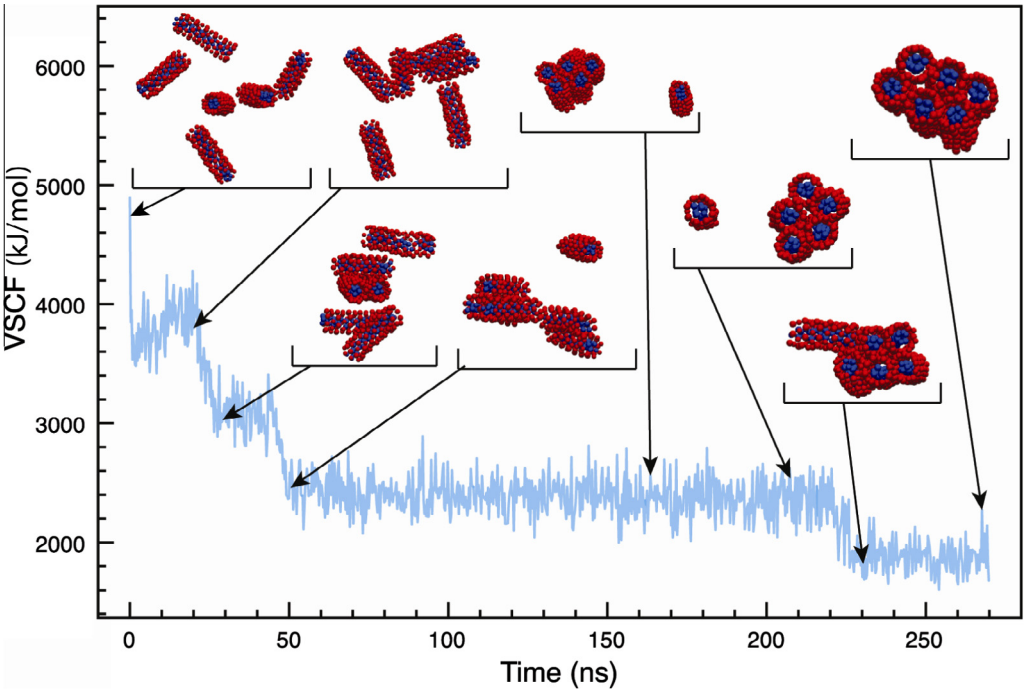


**Figure 1.** Time evolution of particle-field potential (first addend of Eq. (1)) together with some snapshots.

### 3.2. Bundles insertion into lipid bilayers

In Figure 3A the evolution of the center of mass position and orientation of a bundle of six CNTs with length 4.6 nm are reported. In particular, for the system II in Figure 3, and for all the other systems reported in the present Letter, the position along the $z$ axis of the center of mass of the bundle is reported considering as origin the average $x$ coordinate of phospholipids in the first layer. The orientation of the CNT bundle, as schematized in Figure 2A, is calculated considering the angle of the bundle axis with respect to the $z$ direction perpendicular to the bilayer plane. In particular, the order parameter $P_2(t)$ has been calculated from the second order Legendre polynomial $P_2(t) = \frac{3}{2}\cos^2(\theta(t)) - \frac{1}{2}$. Values of $P_2$ close to unity indicate parallel or antiparallel orientations; values close to $-0.5$ indicate a perpendicular orientation. The orientation is measured with respect to the z axis perpendicular to the bilayer plane. According to this definition values of $P_2$ close to unity indicate bundles perpendicular to the bilayer plane, for the same reason values close to $-0.5$ correspond to bundles parallel to the bilayer plane.

As shown in Figure 3A, from the beginning of the MD simulation there is a decrease of the CNT height toward the hydrophobic region of the lipid bilayer. In particular, after about 120 ns the insertion of the CNT bundle inside the hydrophobic region is completed. As shown in Figure 3C, there is no strong correlation between CNT height with respect to the lipid bilayer and its orientation. Due to the low aspect ratio of the CNTs (their length is 4.6 nm) the orientation of the CNT bundle is very variable. During the simulation the particle-field potential reported in Figure 3B shows a fast and monotonic decrease up to 150 ns. These results are consistent with the ones obtained by Lelimousin and Sansom for short single CNTs inserting into lipid bilayers [27].

In order to analyze the distortions of the lipid bilayer during the insertion process, two geometrical quantities have been considered. In particular, the deviation from the equilibrium lipid height ($\Delta z$) and the value of the cosine of the angle $\theta$ between the lipid

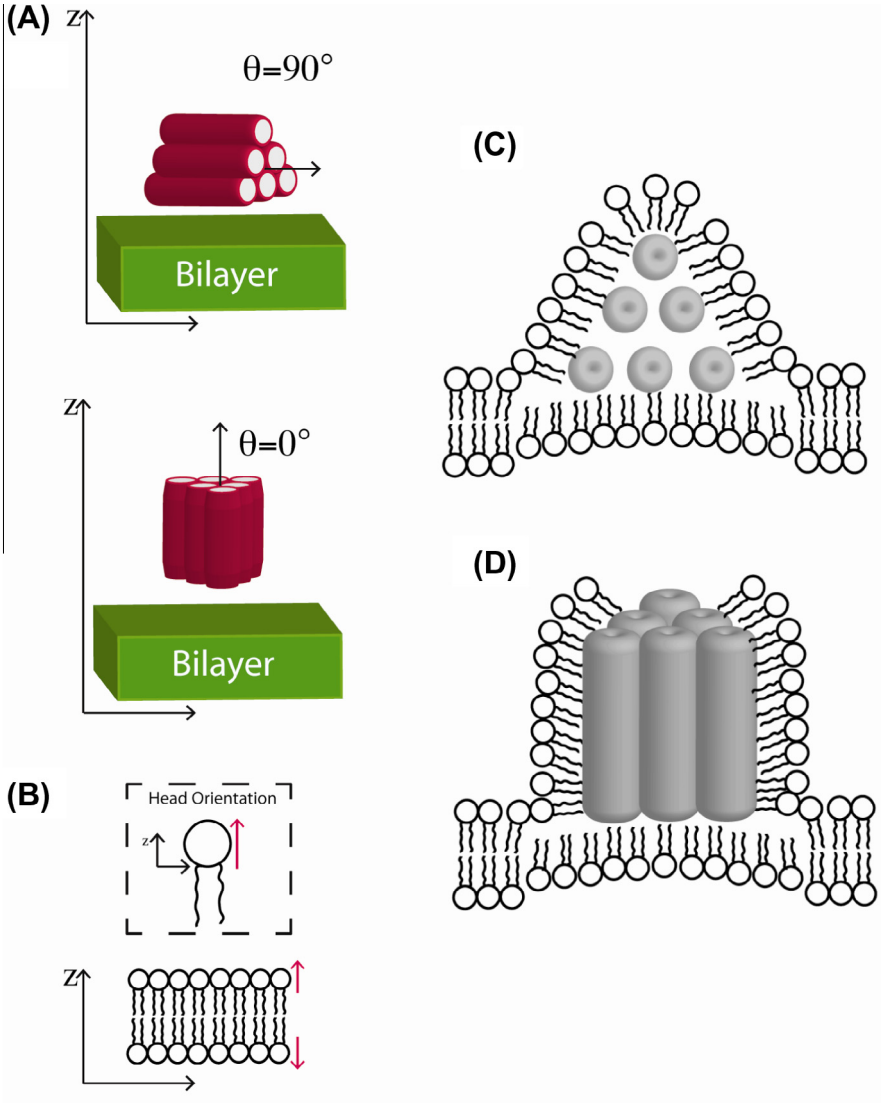


**Figure 2.** Definition of: (A) CNT bundle orientation with respect to $z$ axis perpendicular to the lipid bilayer plane. The orientation is measured with respect to the $z$ axis according to this definition values of $P_2$ close to unity indicate bundles perpendicular to the bilayer plane, for the same reason values close to $-0.5$ correspond to bundles parallel to the bilayer plane. (B) Orientation of lipid molecules with respect to the bilayer plane. A vector (depicted in red) joining beads of type G and N (the bead definition is reported in a previous paper at the Ref. [38]) is used to define the orientation along the $z$ axis. Typical orientations of lipids during the insertion process of a CNT bundle in parallel (C) and perpendicular (D) orientation with respect to the bilayer plane. (For interpretation of the references to color in this figure legend, the reader is referred to the web version of this article.)

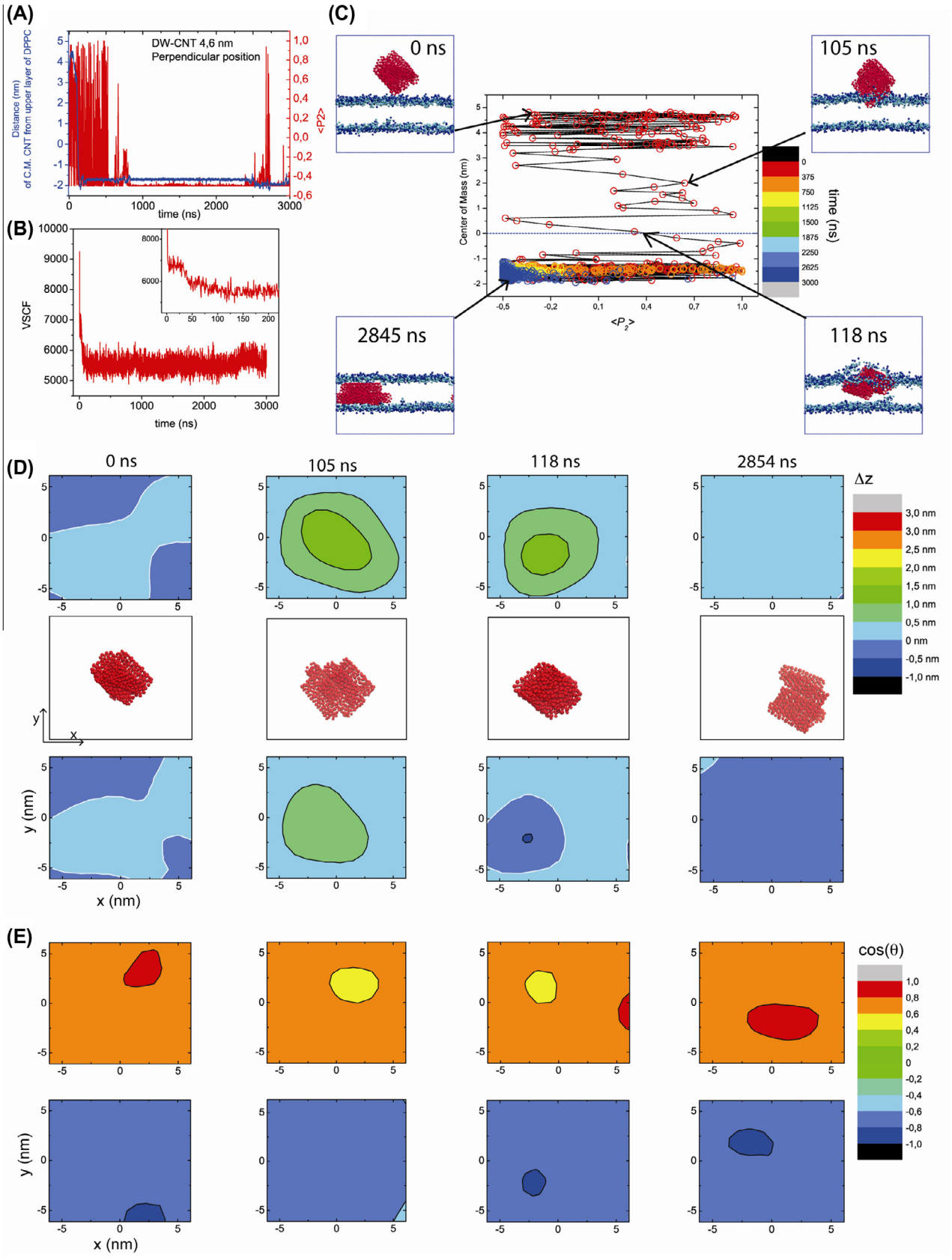


**Figure 3.** System II: Time behavior of (A) CNT bundle center of mass height (blue curve) and orientation with respect the $z$ axis (perpendicular to the bilayer plane, $P_2$, red curve); (B) Particle field potential (sum over particles of the first addend of Eq. (1)); (C) Correlation between center of mass height and bundle orientation together with some snapshots of the system; (D) Deviation ($\Delta z$) from the equilibrium height for upper (top of figure) and lower lipid layers (bottom of figure) for different configurations In the center of figure (D) the corresponding configurations of CNT bundle are depicted. (E) Lipid orientation $\cos\theta$. Both $\Delta z$ and $\cos\theta$ have been averaged on a lattice made of $8 \times 8$ cells. In every cell, on average, there are 6.5 lipids/layer. (For interpretation of the references to color in this figure legend, the reader is referred to the web version of this article.)

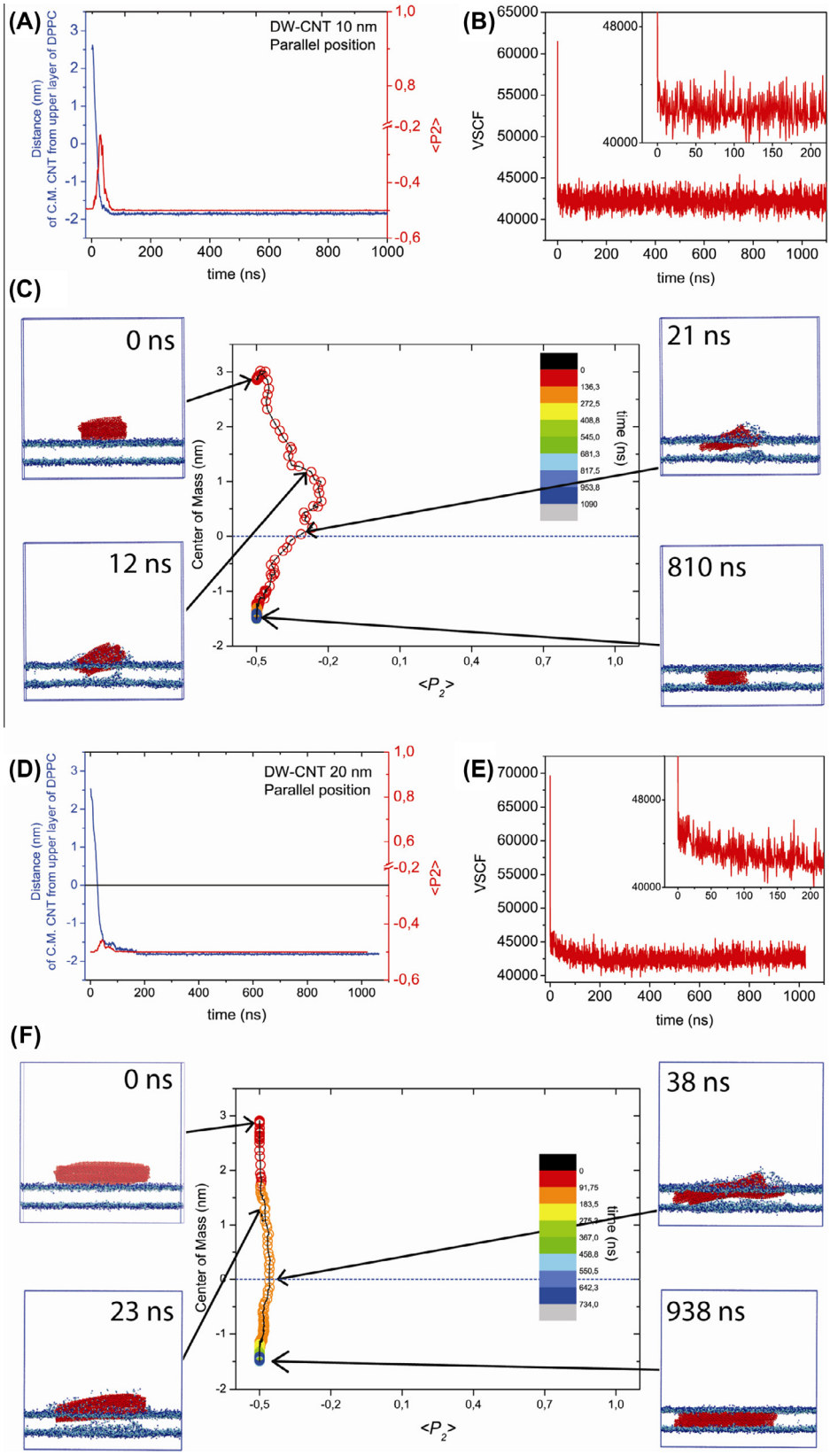


**Figure 4.** Bundle in parallel orientation: System III (A–C). Time behavior of (A) DWCNT-10 nm bundle center of mass height (blue curve) and orientation (with respect to $z$ axis perpendicular to the bilayer plane, $P_2$, red curve); (B) Particle field potential (sum over all particles of first addend of Eq. (1)); (C) Correlation between center of mass height and bundle orientation together with some snapshots. System IV (D–F). Time behavior of (D) DWCNT-20 nm bundle center of mass height and orientation; (E) Particle field potential. (F) Correlation between center of mass height and bundle orientation together with some snapshots. (For interpretation of the references to color in this figure legend, the reader is referred to the web version of this article.)

and the $z$ axis as defined in Figure 2B are considered. In Figure 3D the deviation from the equilibrium height for upper (top panel of Figure 3D) and lower layers of lipids (bottom panel of Figure 3D) and the orientation of DPPC molecules with respect to the $z$ axis in the upper (top of panel of Figure 3E) and lower layers (bottom of panel of Figure 3E), as defined in Figure 2B, are reported for different configurations. In the center the corresponding configurations of CNT bundle are depicted in Figure 3D. As shown in the plots of Figure 3D, the larger perturbation on the lipids height on both upper and lower layers is obtained between 105 and 118 ns, during the insertion process of the CNT bundle with a deviation in the lipids height between 1 and 1.5 nm. This behavior becomes clearer by comparing the plots of Figure 3D and the simulation snapshots reported in Figure 3C. A similar behavior is obtained for the lipids orientation, in particular, as shown in Figure 3E in the upper layer in a region localized close to the CNT bundle, for configurations between 105 and 118 ns, where the lipid orientation is about 90° with respect to the $z$ axis. When the CNT bundle approaches the lipid bilayer large distortion of the lipids heights and orientation occurs. The lipids closer to the CNTs of the bundles tend to be adsorbed on the CNT surface and to orient pointing the hydrophobic carbon tails towards and to expose the polar heads to the water phase. As shown in the following, this is a common process in all the considered systems. A schematization of this behavior is depicted in Figure 2C and D. Results summarized in Figure 3 are similar to the ones reported by Lelimousin and Sansom [27] for the insertion of single CNTs and by Baoukina et al. [28] for the insertion of bundles made of CNTs long 6.5 nm. In particular, distortion of lipid height and orientations have been found during the insertion process in the region close to the bundle, but the membrane integrity is preserved during the insertion process.

In the following, simulation results involving four systems having CNT bundles of larger aspect ratios are reported. In particular, the insertions of bundles made of CNT of length 10 and 20 nm starting from parallel and perpendicular orientations of the bundle axis with respect to the bilayer plane have been simulated.

In Figure 4 the main features of the insertion process bundles made of CNTs of length 10 (system III) and 20 nm (system IV) in parallel orientation are summarized. Similarly to the system with shorter CNTs, from the beginning of the MD simulation there is a decrease of the CNT height toward the hydrophobic region of the lipid bilayer. Differently from the system with shorter CNTs, where basically no correlation between bundle height and its orientation is found, here a parallel orientation with some deviations larger for the system with CNTs of length 10 nm (Figure 4C) and very small for the systems with CNTs of length 20 nm (Figure 4F). In both cases, during the simulation the intermolecular potential (first addend of Eq. (1) in the particle-field approximation) shows a fast

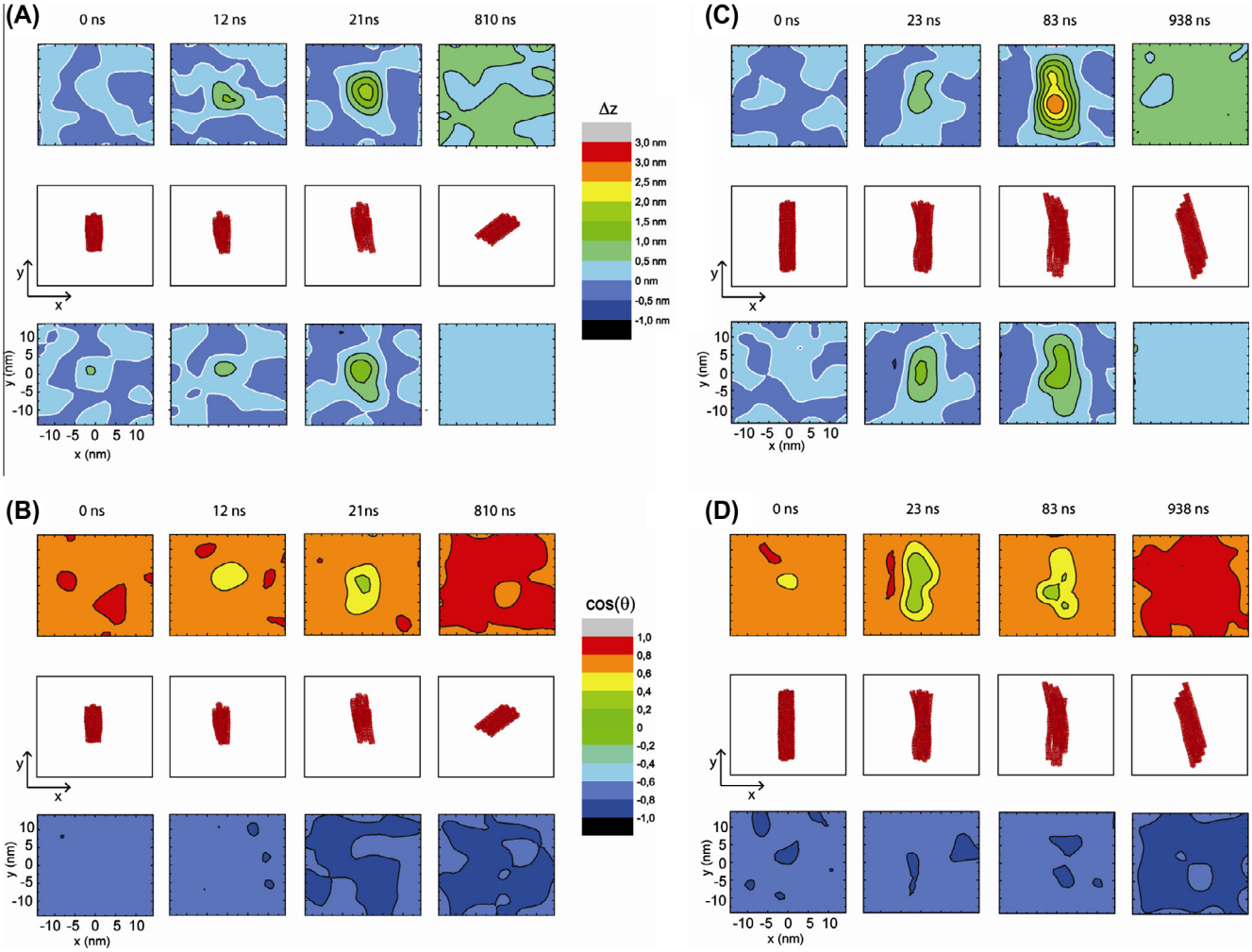


**Figure 5.** Deviation $\Delta z$ (A, C) and Lipid orientation $\cos\theta$ for the systems III and IV with bundle CNT in parallel orientation. (A) deviation $\Delta z$ from the equilibrium height for upper (top of the panel) and lower lipid layers (bottom panel) for different configurations of system III. (C) Deviation $\Delta z$ for system IV. (B) Lipid orientation $\cos\theta$ for system III. (D) Lipid orientation $\cos\theta$ for system IV. In the center of each figure (A–D), the corresponding configurations of CNT bundle are depicted. Both $\Delta z$ and $\cos\theta$ have been averaged on a lattice made of $16 \times 16$ cells (with the same cell size, about 2 nm, of the system II). In every cell, on average, there are 6.5 lipids/layer.

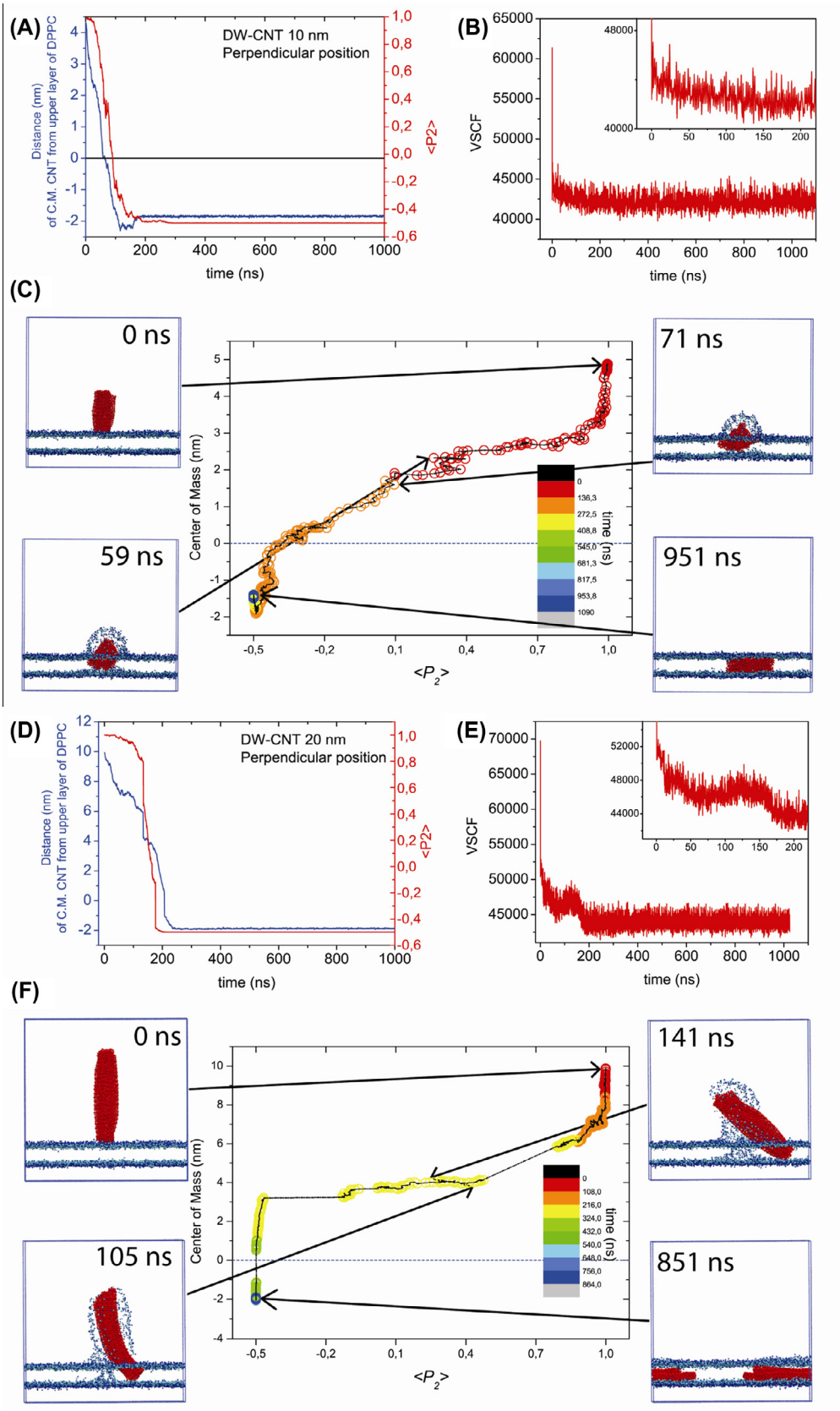


**Figure 6.** Bundle in perpendicular orientation: System III (A–C). Time behavior of (A) DWCNT-10 nm bundle center of mass height (blue curve) and orientation (with respect to $z$ axis perpendicular to the bilayer plane, $P_2$, red curve); (B) Particle field potential (sum over all particles of first addend of Eq. (1)); (C) Correlation between center of mass height and bundle orientation together with some snapshots. System IV (D–F). Time behavior of (D) DWCNT-20 nm bundle center of mass height and orientation; (E) Particle field potential. (F) Correlation between center of mass height and bundle orientation together with some snapshots. (For interpretation of the references to color in this figure legend, the reader is referred to the web version of this article.)

and monotonic decrease. The position of the CNT center of mass shows the same behavior and reaches the equilibrium value at ∼−2 nm (i.e. in the central part of the lipid bilayer, the DPPC bilayer thickness is ∼4 nm) in about 50 ns for the bundle having CNTs long 10 nm (Figure 4A) and about 200 ns for the bundle having longer CNTs (20 nm, Figure 4D). In the Figure 5 the distortion of the height and orientation of the lipids for different snapshots taken during the insertion process of the systems III and IV are reported. For both systems, the distortion of equilibrium height of lipids is larger than the one obtained for system II having shorter CNTs (4.6 nm). In particular, for system III in the snapshot showing larger values of $\Delta z$ (Figure 5A, plot at 21 ns) there is a small region with values larger than 2 nm. The insertion process of for system IV causes larger values of $\Delta z$, in particular, in the snapshot showing larger deviations (Figure 5C, plot at 83 ns) there is an extended region having distortions going from 2 up to 3 nm.

Similar is the behavior of lipid orientation during the insertion process. Also in this case both systems III and IV are more perturbed with respect to the one with shorter CNTs, in particular, the region where the orientation is almost perpendicular is larger with a central part where the average value of the $\cos\theta$ is zero.

In Figure 6 the insertion process bundles made of CNTs of length 10 (system III) and 20 nm (system IV) in perpendicular orientation is summarized. Although the process is slower, also in this case, it is possible to observe spontaneous insertion. Comparing the plots of Figure 6C (system III) and Figure 6F (system IV) and the snapshots reported in them it is possible to observe that, for both CNTs lengths, the insertion involves mechanism a concerted insertion/rotation of the bundle. The perturbation of both lipid heights with a region with $\Delta z$ from 1 to 3 nm for the system having CNTs long 10 nm (Figure 7A), and from 1 to 6 nm for the system having CNTs long 20 nm (Figure 7C), and orientation (strong perpendicular orientation, Figure 7B and D) is more localized but stronger than the one obtained with the bundles in parallel orientation.

The insertion process involving a CNT bundle in perpendicular orientation is the one showing the largest perturbation on the structure of the lipid bilayer for both system III and system IV. Moreover, in these cases, the range of perturbation is larger; in particular, large deviations of lipid height are obtained also for the lower lipid layers. An interesting aspect, due to this feature, is the formation of a transient pore in the lipid bilayers during the insertion process of the CNT bundles. In particular, as shown in Figure 8A (system III) and Figure 8C (system IV), starting from the configuration at about 20 (for system III) and 120 ns (system IV) a poration inside the bilayer can be observed. In Figure 8 water beads are reported in yellow. Moreover, in the Figure 8 snapshots corresponding to the maximum size of the pore (at 122 and 145 ns for systems III and IV, respectively) are also reported. It is worth noting that, differently from the other systems considered here, in this case of the insertion in perpendicular orientation for system IV, the particle-field potential (see the behavior reported in Figure 6B and E) does not show a monotonic decrease, but between

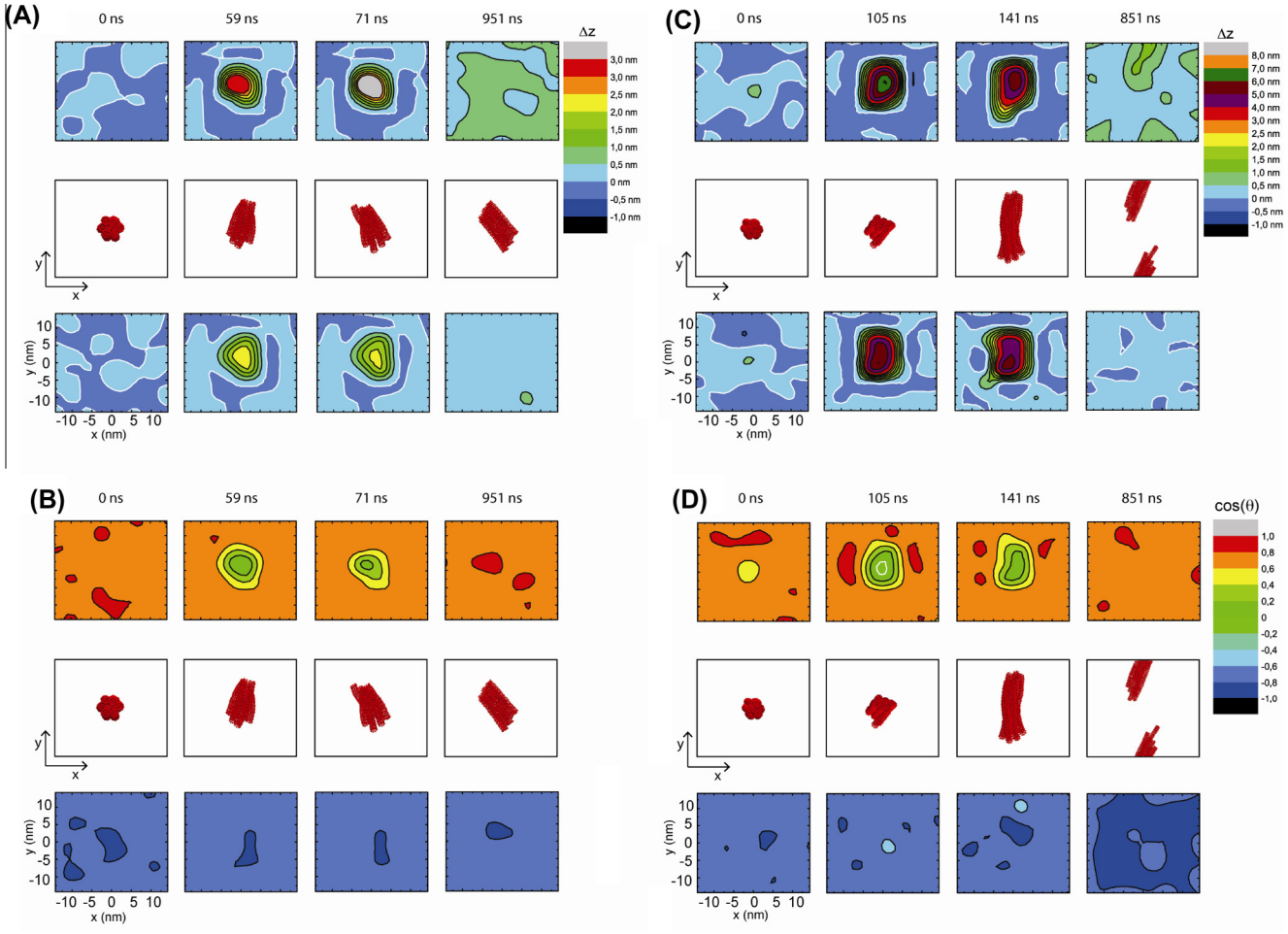


**Figure 7.** Deviation $\Delta z$ (A, C) and Lipid orientation $\cos\theta$ for the systems III and IV with bundle CNT in perpendicular orientation. (A) Deviation $\Delta z$ from the equilibrium height for upper (top of the panel) and lower lipid layers (bottom panel) for different configurations of system III. (C) Deviation $\Delta z$ for system IV. (B) Lipid orientation $\cos\theta$ for system III. (D) Lipid orientation $\cos\theta$ for system IV. In the center of each figure (A–D), the corresponding configurations of CNT bundle are depicted. Both $\Delta z$ and $\cos\theta$ have been averaged on a lattice made of 16 × 16 cells (with the same cell size, about 2 nm, of the system II). In every cell, on average, there are 6.5 lipids/layer.

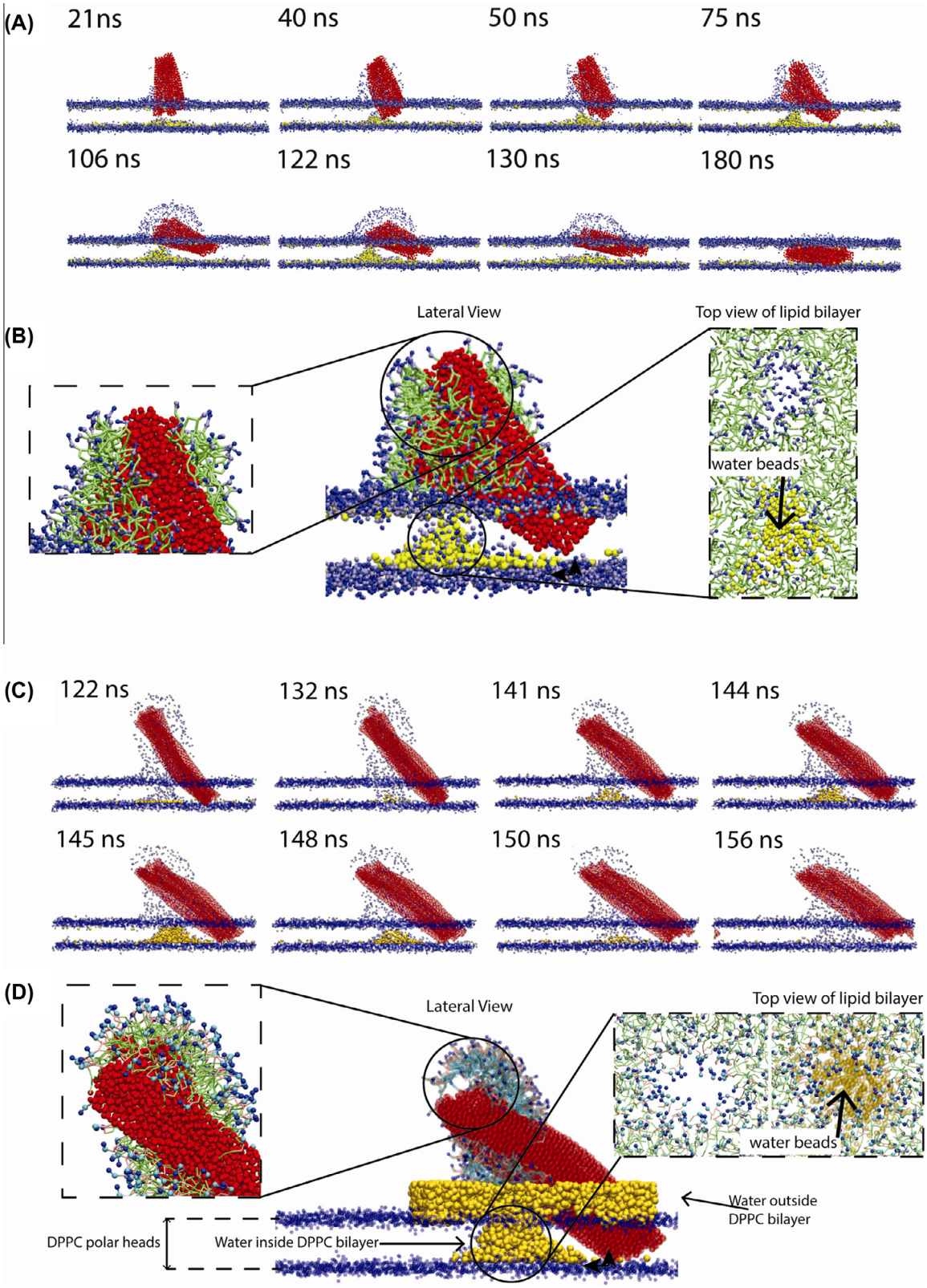


**Figure 8.** Process of pore formation inside the lipid bilayer during the insertion process of a bundle made of CNTs long 10 nm (A) and 20 nm (C). The lipid orientations corresponding to micelle in water around the CNTs (inset on the left side) and reverse micelle (around the pore including water) aggregates (right side) are highlighted for both bundles lengths: (B) 10 nm, (D) 20 nm.

100 and 200 ns shows a local maximum. Interestingly, for this system, the simulation time where the pore size is larger corresponds to the maximum of particle-field potential (see Figure 6C). In the Figure 8B and D the structures of the water pore and the arrangement of lipids on the CNTs surface and around the pore percolated by water is highlighted. In particular, the arrangement on CNT

surface is typical of phospholipids at low concentration in water (micellar phases), due to the process of lipids adsorption on the CNTs surfaces, the number of lipids in the bilayer starts to be low and the poration favorable. As shown in Figure 8, water molecules penetrate in the hydrophobic part of the bilayer and the lipid orientation around the water rich region is of reverse micelle type (hydrophilic heads are exposed to water and hydrophobic tails point to the unperturbed region). Snapshots showing the coating process of lipids toward the CNT surfaces are reported in Figure 2 of the supporting material.

## 4. Conclusions

In all considered systems it has been possible to observe spontaneous insertion of bundles made of CNTs of different lengths ranging from 4.6 to 20 nm. In all cases the insertion process causes distortions in both lipid height and orientation. In particular, during the insertion process lipid molecules tend to coat bundles surfaces and this causes an increase of the average lipids heights in both upper and lower lipid layers. The lipids closer to the bundle tend to orient their carbon tails toward the hydrophobic surfaces of CNTs. These distortions are more pronounced for systems having long CNTs and oriented perpendicularly to the bilayer surfaces. In all cases these distortions are transient and they become minimal when the CNTs forming the bundle rearrange inside the hydrophobic region of the lipid bilayers. The results involving short CNTs are in agreement with previously reported simulation studies using CG models [27,28] Using the hybrid PF methodology, it has been possible to extend the range of applicability of MD simulations. Hybrid PF models allowed to study the entire process of spontaneous insertions of bundles made of longer CNTs (10 and 20 nm). Interestingly, in this case, due to the larger systems size, bundles made of longer CNTs, when the insertion occurs in perpendicular orientation, promote a transient poration. This result can be an indication of a possible mechanism of membrane disruption operated by CNTs bundles causing the formation of solvent-rich pockets.

## Acknowledgments

G.M. thanks MIUR (FIRB 'RETE ITALNANONET') for financial support and the HPC team of Enea (http://www.enea.it) for using the ENEA-GRID and the HPC facilities CRESCO (http://www.cresco.enea.it) in Portici.

## Appendix A. Supplementary data

Supplementary data associated with this article can be found, in the online version, at http://dx.doi.org/10.1016/j.cplett.2014.01.057.

## References

[1] L. Lacerda, A. Bianco, M. Prato, K. Kostarelos, Adv. Drug Deliv. Rev. 58 (2006) 1460.
[2] K. Kostarelos, L. Lacerda, G. Pastorin, W. Wu, NANO 2 (2007) 108.
[3] Y. Wenrong, T. Pall, J.J. Gooding, P.R. Simon, B. Filip, Nanotechnology 18 (2007) 412001.
[4] N. Sinha, J.T.W. Yeow, IEEE Trans. Nanobiosci. 4 (2005) 180.
[5] D. Pantarotto, J.-P. Briand, M. Prato, A. Bianco, Chem. Commun. (2004) 16.
[6] D. Pantarotto et al., Angew. Chem. 116 (2004) 5354.
[7] N.W.S. Kam, Z. Liu, H. Dai, J. Am. Chem. Soc. 127 (2005) 12492.
[8] M. Foldvari, M. Bagonluri, Biol. Med. 4 (2008) 183.
[9] C. Tripisciano, K. Kraemer, A. Taylor, E. Borowiak-Palen, Chem. Phys. Lett. 478 (2009) 200.
[10] G.R. Liu, Y. Cheng, D. Mi, Z.R. Li, Int. J. Mod. Phys. C 16 (2005) 1239.
[11] Y. Kang, Y.-C. Liu, Q. Wang, J.-W. Shen, T. Wu, W.-J. Guan, Biomaterials 30 (2009) 2807.
[12] K.T. Al-Jamal et al., Nanoscale 3 (2011) 2627.
[13] A.E. Porter et al., ACS Nano 3 (2009) 1485.
[14] A.E. Porter, M. Gass, K. Muller, J.N. Skepper, P.A. Midgley, M. Welland, Nat. Nano 2 (2007) 713.
[15] F. Zhou, D. Xing, B. Wu, S. Wu, Z. Ou, W.R. Chen, Nano Lett. 10 (2010) 1677.
[16] C. Lamprecht et al., Nanotechnology 20 (2009) 434001.
[17] V.K. Gangupomu, F.M. Capaldi, J. Nanomater. 2011 (2011) 6.
[18] S. Höfinger, M. Melle-Franco, T. Gallo, A. Cantelli, M. Calvaresi, J.A.N.F. Gomes, F. Zerbetto, Biomaterials 32 (2011) 7079.
[19] P.N. Yaron, B.D. Holt, P.A. Short, M. Losche, M.F. Islam, K.N.J. Dahl, J. Nanobiotechnol. 9 (2011) 45.
[20] V. Raffa, G. Ciofani, O. Vittorio, C. Riggio, A. Cuschieri, Nanomedicine 5 (2009) 89.
[21] R. Parthasarathi, N.R. Tummala, A. Striolo, J. Phys. Chem. B 116 (2012) 12769.
[22] Y. Tu et al., Nat. Nano 8 (2013) 594.
[23] C.F. Lopez, S.O. Nielsen, P.B. Moore, M.L. Klein, Proc. Natl. Acad. Sci. USA 101 (2004) 4431.
[24] R. DeVane, A. Jusufi, W. Shinoda, C.-C. Chiu, S.O. Nielsen, P.B. Moore, M.L. Klein, J. Phys. Chem. B 114 (2010) 16364.
[25] J. Wong-Ekkabut, S. Baoukina, W. Triampo, I.M. Tang, D.P. Tieleman, L. Monticelli, Nat. Nano 3 (2008) 363.
[26] S. Pogodin, V.A. Baulin, ACS Nano 4 (2010) 5293.
[27] M. Lelimousin, M.S.P. Sansom, Small (2013) 3639.
[28] S. Baoukina, L. Monticelli, D.P. Tieleman, J. Phys. Chem. B 117 (2013) 12113.
[29] A. Magrez et al., Nano Lett. 6 (2006) 1121.
[30] G. Milano, T. Kawakatsu, J. Chem. Phys. 130 (2009) 214106.
[31] K.M. Langner, G.J.A. Sevink, Soft Matter 8 (2012) 5102.
[32] M. Mueller, K. Katasov, M. Schick, Phys. Rep. 434 (2006) 113.
[33] G. Milano, T. Kawakatsu, A. De Nicola, Phys. Biol. 10 (2013) 045007.
[34] M. Homberg, M. Muller, J. Chem. Phys. 132 (2010) 155104.
[35] G.J.A. Sevink, M. Charlaganov, J.G.E.M. Fraaije, Soft Matter 9 (2013) 2816.
[36] K.C. Daoulas, M. Muller, J. Chem. Phys. 125 (2006) 184904.
[37] K.C. Daoulas, M. Muller, J.J. de Pablo, P.F. Nealey, G.D. Smith, Soft Matter 2 (2006) 573.
[38] G. Milano, T. Kawakatsu, J. Chem. Phys. 133 (2010) 214102.
[39] A. De Nicola, Y. Zhao, T. Kawakatsu, D. Roccatano, G. Milano, J. Chem. Theory Comput. 7 (2011) 2947.
[40] A. De Nicola, Y. Zhao, T. Kawakatsu, D. Roccatano, G. Milano, Theoret. Chem. Acc. 131 (2012) 1167.
[41] Y. Zhao, A. De Nicola, T. Kawakatsu, G. Milano, J. Comput. Chem. 33 (2012) 868.